symmetry

MDPI

Article

Deep Convolutional Neural Network Based Analysis of Liver Tissues Using Computed Tomography Images

Mehrun Nisa [1,2], Saeed Ahmad Buzdar [2], Khalil Khan [3,*] and Muhammad Saeed Ahmad [4]

[1] Department of Physics, Govt. Sadiq College Women University, Bahawalpur 63100, Pakistan; mehr.phy@gscwu.edu.pk
[2] Institute of Physics, The Islamia University of Bahawalpur, Bahawalpur 63100, Pakistan; saeed.buzdar@iub.edu.pk
[3] Department of Information Technology and Computer Science, Pak-Austria Fachhochschule Institute of Applied Sciences and Technology, Haripur 22620, Pakistan
[4] Department of Computer Science and Information Technology, Govt. Sadiq College, Women University, Bahawalpur 63100, Pakistan; drsaeed@gscwu.edu.pk
* Correspondence: khalil.khan@fecid.paf-iast.edu.pk

Abstract: Liver disease is one of the most prominent causes of the increase in the death rate worldwide. These death rates can be reduced by early liver diagnosis. Computed tomography (CT) is a method for the analysis of liver images in clinical practice. To analyze a large number of liver images, radiologists face problems that sometimes lead to the wrong classifications of liver diseases, eventually resulting in severe conditions, such as liver cancer. Thus, a machine-learning-based method is needed to classify such problems based on their texture features. This paper suggests two different kinds of algorithms to address this challenging task of liver disease classification. Our first method, which is based on conventional machine learning, uses texture features for classification. This method uses conventional machine learning through automated texture analysis and supervised machine learning methods. For this purpose, 3000 clinically verified CT image samples were obtained from 71 patients. Appropriate image classes belonging to the same disease were trained to confirm the abnormalities in liver tissues by using supervised learning methods. Our proposed method correctly quantified asymmetric patterns in CT images using machine learning. We evaluated the effectiveness of the feature vector with the K Nearest Neighbor (KNN), Naive Bayes (NB), Support Vector Machine (SVM), and Random Forest (RF) classifiers. The second algorithm proposes a semantic segmentation model for liver disease identification. Our model is based on semantic image segmentation (SIS) using a convolutional neural network (CNN). The model encodes high-density maps through a specific guided attention method. The trained model classifies CT images into five different categories of various diseases. The compelling results obtained confirm the effectiveness of the proposed model. The study concludes that abnormalities in the human liver could be discriminated and diagnosed by texture analysis techniques, which may also assist radiologists and medical physicists in predicting the severity and proliferation of abnormalities in liver diseases.

Keywords: liver disease classification; deep learning; semantic image segmentation

Citation: Nisa, M.; Buzdar, S.A.; Khan, K.; Ahmad, M.S. Deep Convolutional Neural Network Based Analysis of Liver Tissues Using Computed Tomography Images. *Symmetry* **2022**, *14*, 383. https://doi.org/10.3390/sym14020383

Academic Editors: Chien-Hsing Chou and Yi-Zeng Hsieh

Received: 13 January 2022
Accepted: 6 February 2022
Published: 15 February 2022

1. Introduction

The liver is an essential organ with a weight of nearly 1.5 kg and making up 2% of the mass of the whole body. The liver performs significant life-sustaining functions. The physiological roles of the liver are divided into those of hepatic sinusoids and hepatocytes. The liver is called the chemical plant of the body [1]. According to a report by the WHO, 62.6% of deaths are due to liver diseases, of which 54.3% are due to cirrhosis; more than two-thirds of the world's problems with the disease acute hepatitis occur in this particular area [2]. According to a WHO report [3], in the region of Asia, cirrhosis is the prominent cause of death due to liver diseases. In 2016, nearly 399,000 people died due to different

liver diseases, e.g., cirrhosis, hepatocellular carcinoma, and hepatitis C. The WHO has made a strategy to declare liver disease a public health problem.

The last several decades have shown that abnormalities such as liver abscesses are sometimes severe and are subject to substantial epidemiological changes and risk factors [4]. The most common liver abscesses are caused by blood infections, abdominal infections, infections due to injury, and bacterial or parasitic infections. To avoid complications in untreated patients, it is essential to recognize the abscesses' severity, diagnosis, and treatment. The significant sources of pyogenic liver abscesses are biliary tract diseases [5]. Hypoxia, ischemia, drug exposure, and infection cause damage to the liver. However, damaged cells cannot recover after a specific limit, leading to permanent damage. Sometimes, this generates scar tissue or non-functioning cells in the liver, which is called fibrosis [6]. Until the 1970s, liver fibrosis and cirrhosis were considered irreparable. Cirrhosis was first discussed in the literature in 1819 by Laennec as a primary cancer that could be seen in the liver by its colors [7]. Liver cirrhosis is the next stage of fibrosis caused by liver diseases such as liver injury, swelling, abnormal growth of non-functioning cells, and angiogenesis [8]. Secondary liver cancer or a metastatic hepatic tumor is more noticeable than a primary tumor. About 70% to 80% of metastatic liver cancer cases remain limited to the liver [9]. Liver metastases typically hypo-attenuate in un-enhanced CT. If there is concomitant hepatic steatosis, the lesions may be isolated or slightly hyper-attenuated.

Necrosis, also known as cell death or the death of bodily tissues, is when viable cells become nonviable, resulting in a suspension of the cell contents. This occurs when too little blood is supplied to the tissues. It is an irreversible process caused by injury, radiation, or chemical effects. Necrosis is found in chronic liver disease, and with the persistence of its underlying cause, it is followed by a progressive disease—fibrosis [3]. Thus, the extent of necrosis is a part of the information collected from a biopsy. The extent of necrosis ranges from individual cells to massive hepatic cases. The pathologist's role is to evaluate the pattern of tumors in the context of some morphological changes in order to suggest one or more possible underlying causes [10]. In other cases, most of the liver's vascular disorders are uncommon, except for portal vein thrombosis (PVT). Most patients can easily establish PVT diagnoses through a process called noninvasive imaging [11]. After liver cirrhosis, the second leading cause of portal hypertension is PVT. Liver cirrhosis, hepatobiliary malignancy, inflammatory diseases, and thrombophilic disorders, including myeloproliferative diseases, are intensely concomitant with PVT development [7].

In combination, homogeneous and heterogeneous patterns or frequency levels make a texture. Texture can be visualized, but it is more concrete to explain its statistical parameters. Liver texture demonstrates a similar nature. The micro-changes in intensity levels in a liver's texture on the inside and along boundaries with other organs can produce severe problems in discriminating liver abnormalities [8].

We searched Web of Science, the Google Scholar database, PubMed, and EMBASE to identify relevant articles published to date on liver disease diagnosis. We used keywords such as liver disease diagnosis using machine learning, texture analysis, computed tomography, computer-aided diagnosis, etc. We noticed early research work on the topic with limited datasets and methodologies. Most of these datasets are also not publicly available. For this reason, we collected our own dataset consisting of around 3000 CT images, which is the main contribution of this paper. Some relevant articles that we found on the topic are listed in [12–18].

We noticed that the primary task in liver diagnosis and treatment is to visualize the texture of the patient. However, it is impossible to read all of the patient's information in an image with a naked eye. Briefly, there can be many errors in the information collected for diagnoses from patients' images due to homogeneity and heterogeneity in texture patterns. Different statistical methods and mathematical techniques can be adopted to attain accuracy in diagnostic imaging, and there are also various ways to extract texture features. The Haralick texture features include the Sum Average, Angular Second Moment, Sum Variance, Difference Variance, Inverse Difference Moment, Difference Entropy, and Infor-

mation Measures of Correlation, Contrast, and Correlation. A Gray-Level Co-Occurrence Matrix (GLCM) was constructed in the proposed work. A GLCM contains second-order statistics for retrieving pixels' information from a gray-level distribution within the ROIs, as introduced by Haralick et al. [19].

The research work presented in this paper targets the assessment of the effectiveness of texture analysis through machine learning for differentiation among five different classes. We propose two methods for liver disease recognition using deep convolutional networks and conventional machine learning methods. Only two or three texture models of liver images have been considered to date. Hence, in our present article, we consider the quantitative evaluation of seven different kinds of texture models for liver CT images. We extracted 37 features from the models and then provided specially mined features for different feature selections. We also used the feature-ranking method to investigate the best settings.

2. Related Work

Liver disease classification using ML is not a new research area. Many good papers on the topic have been published by researchers. We searched Web of Science, the Google Scholar database, PubMed, and EMBASE to identify relevant articles published to date on liver disease diagnosis. We used keywords such as liver disease diagnosis using machine learning, texture analysis, computed tomography, computer-aided diagnosis, etc. We noticed early research work on the topic with limited datasets and methodologies. Most of these datasets are also not publicly available. For this reason, we collected our own dataset consisting of around 3000 CT images, which is the main contribution of this paper. Some relevant articles that we found on the topic are listed in [12–18].

ML experts have explored neural networks, SVM, decision trees (DT), and other ML models to investigate this problem. This part of the paper discusses some of these methods that explore liver disease classification. The authors of [20] implemented methods such as J48, NB, random tree (RT), and K-star. Another paper [21] used algorithms such as logistic regression, RT, and SVM for classification. A back-propagation network (BPN) combined with a multilayer feed-forward deep neural network (MLFFDNN) was utilized by [22]. XGBoost was used to estimate liver disease data, and the authors used L1 and L2 [23] during their work. An imbalance in ILPD was handled through a specific method called the minority oversampling algorithm. The performance was assessed for balanced and unbalanced databases with SVM and KNN [24].

Another method that explored particle swarm optimization (PSO) combined with SVM for feature selection was investigated in [25]. Comparatively good results were reported with the use of an SVM classifier [25]. Heuristic and nature-inspired meta-heuristic optimization algorithms (MHOAs) improved the performance of the method. The classification accuracy was furhter improved with methods such as grid search and the Nelder–Mead method [26].

The Grasshopper [27] and Firefly algorithms [28] improved the accuracy in combination with SVM. However, these algorithms were still found to have some limitations. Another method that combined the Crow Search Optimization Algorithm (CSA) with SVM was reported in [29]. According to the authors of the paper, the method proposed in [29] maintained a balance between exploitation and exploration. The method proposed in [29] had two parameters. The method was fast and straightforward to implement.

3. Liver CT Image Database

The significant contribution of the proposed paper is the collection of a database of liver images with normal and infected data. Very few tiny datasets have been reported in the literature regarding liver disease classification through machine learning. For this research, clinically verified CT imaging data were collected from the Bahawal Victoria Hospital, Bahawalpur, Pakistan. The CT machine used X-rays to acquire images with both spiral and sequential methods. Axial reconstruction minimized the averaging of

the lesions as far as partial volume was concerned. Similarly, it also allowed hepatic enhancement scanning in three phases: the portal, arterial, and delayed phases. Moreover, issues regarding registration were minimized due to a process called single-hold breath.

A total of 3000 samples of 71 patients were selected and studied after discussion with the expert radiologists involved in the management. We kept the size of each image at 512 × 512. The scanner on which we obtained images was a 128-slice scanner with a 12-bit depth and a slice thickness varying in the range of 0.6–1 mm. We acquired images in the arterial, delayed, and portal venous phases. We studied five categories of liver images, namely, infected liver data, liver metastasis, tumor necrosis, vascular disorder, and normal liver images. A complete discussion was set up with the doctors' and radiologists' teams in each step. The dataset will be publicly available for research purposes after the publication of our paper.

The inclusion criteria were the collection of data from infected patients with hepatitis B and C, a metastatic tumor (secondary tumor), tumor necrosis, or vascular disorder because of the availability of said data types. Patients on ventilators and renal function tests or who were children were excluded from the current study. Due to the low socioeconomic status of the area, biopsy to the confirm clinical data was impossible for the patients. The gold standard for the final diagnosis was serum alpha-fetoprotein and triphasic multidetector computed tomography of the liver, in which non-ionic intravenous ultravist contrast was used to enhance the diseased pattern. Table 1 shows the demographic data of the patients selected for the study. Figures 1 and 2 show some images of our collected database. Figure 1 shows images with some abnormalities at some stages. Figure 2 compares normal case images with infected data.

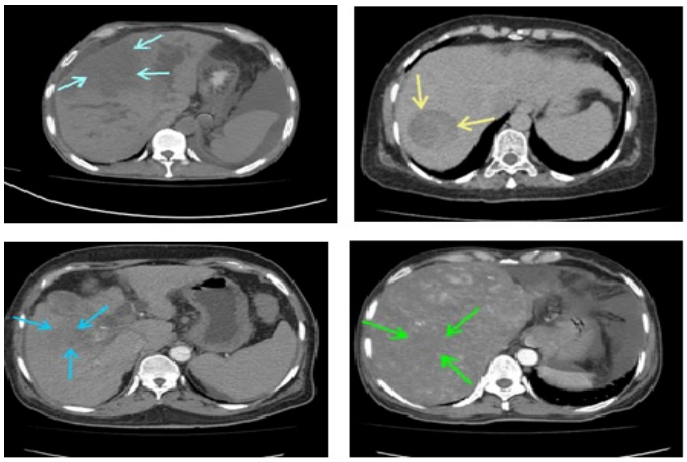

Figure 1. Some sample images were taken from the proposed database. In the images, abnormalities are highlighted in different subjects' livers. Row one shows an infected liver or liver abscess and a metastatic liver, whereas row two shows tumor necrosis and an abnormal vascular area in the liver.

Table 1. Demographic data of the patients.

Number of Patients	Gender	Age Limit	Existing Disease Process/Lesion
19	M-12, F-7	28–56	Abscess infection, hepatitis B, C
15	M-11, F-4	40–70	Metastatic CA colon, gall bladder, prostrate, ovary, and breast
23	M-18, F-5	40–70	Metastatic, necrotic tumor
26	M-16, F-9	40–50	Metastatic, vascular disorder, AV malformation (arteriovenous malformation), hemangioma
16	M-22, F-19	40–50	normal

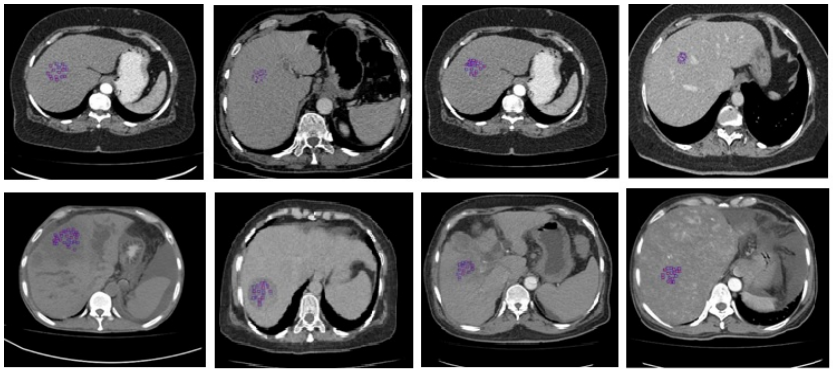

Figure 2. Construction of ROIs for the conventional machine learning methodology. Column 1: CT image of a normal class 1 liver versus an infected liver; column 2: CT image of a normal class 2 liver versus a metastatic liver, column 3: CT image of a normal class 3 liver versus a metastatic liver; column 4: CT image of a normal class 4 liver versus an abnormal vascular area in the liver.

4. Proposed Method

For the implementation of our proposed method, we explored both conventional machine learning and deep-learning-based methods. This section of the paper gives details about both methods. We use two methods in our proposed work. Conventional machine learning method is summarized in Figure 3.

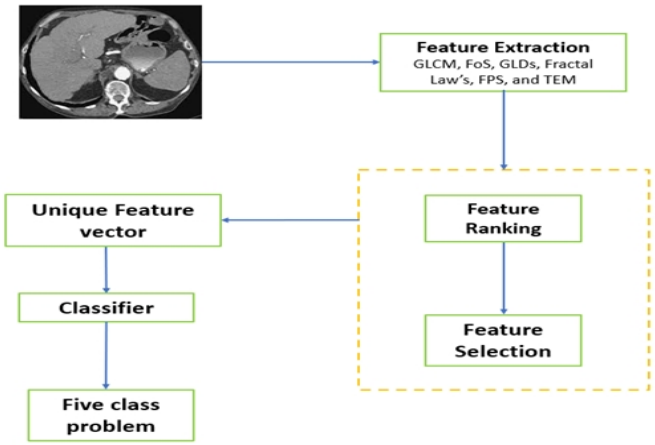

Figure 3. Steps involved in the proposed method.

4.1. ROI Extraction

An ROI is a segment of an image containing details that assist in specific liver diagnoses. n ROI works as an essential image representation for advanced disease diagnoses, so selecting such image regions is an important task. We chose a polygonal ROI that included enough area to collect features from texture models. We used the method suggested in [30].

4.2. Extraction of Features

Feature extraction is a crucial step in any machine learning method, since it identifies essential details about the contents of an image. Different liver lesions show various distinct texture features or patterns; for example, different gray-level intensity patterns and values are shown by images with abnormal and normal conditions. Different models for acquiring texture features have been reported in the literature [31–33]. These models visualize the contents of an image in various ways. Some of these ways are textural details about the spatial distribution of pixel values and derivations from the level of brightness [19].

We used seven models to acquire features from specific ROIs in the proposed work. These features included the First-Order Statistics (FoS) [34], Gray-Level Spatial Co-Occurrence

Matrix (SGLCM) [35,36], Gray-Level Difference Statistics (GLDS) [37], Fourier Power Spectrum (FPS) [38], Fractal Features [39], Statistical Feature Matrix (SFM) [40], and Law's Texture Energy Measures (TEM) [41]. We extracted 37 features from the CT images and then normalized each to have the unit variance and zero means. The texture features extracted are summarized in Table 2.

Table 2. Extracted features used in the proposed work.

Feature Name	Extracted Feature Details
FoS	Median, Mean, Variance, Skewness, Kurtosis
SGLCM	The angular second moment, contrast, sum of squares, inverse difference moment, variance, difference variance, difference entropy, information measure of correlation
GLDS	Homogeneity, contrast, energy, entropy, mean
Law's TEM	LS, ES, LE, SS, LE, LL
Fractal	Hurst coefficients

4.3. Feature Ranking

To remove redundant information, we added feature ranking to our framework. This step went before the classification stage. As most of the features used for a specific disease diagnosis are correlated with each other, feature ranking avoids collinearity, reduces the dimensions of feature vectors, and somehow minimizes noise [42]. For feature ranking using dimensionality power, we applied a filter-based algorithm. We employed knowledge-based feature ranking, the chi-square, gain (ratio and information), and relief feature ranking [43]. These features were explored in the works reported in [44,45].

4.4. Classifier Setting

We performed a validation of the ranked features using various classifiers, including Support Vector Clustering (SVC), which is an extension of the widely used SVM. We used NB, SMO, RF, and KNN by changing various parameters of these classifiers, as shown in Table 3. We also employed LibSVM with three versions: a radial basis function (RBF) kernel, a sigmoid function, and a polynomial. We set the gamma parameters in the cases mentioned to 1.25. We fixed the number of trees in RF to 10. NB-1 had no kernel function for evaluating the distribution of data. NB-2 used KF to evaluate the data distribution. We employed the SMO method for the training of SVM. We performed its implementation with a polynomial function kernel by setting the exponent value to 1 and setting omega and sigma to 1. Similarly, we used the KNN classifier in three versions, and the Euclidean distances were fixed at 6, 7, and 8.

Table 3. Parameter settings of the different classifiers.

Classifier	Classifier Version	Various Parameter Settings
KNN	KNN-1	Value of k fixed at 6 and the function used is Euclidean distance
	KNN-2	Value of k fixed at 7 and the function used is Euclidean distance
	KNN-3	Value of k fixed at 8 and the function used is Euclidean distance
LibSVM	LibSVM-1	Radial basis function kernel and gamma = 1.25, whereas c = 1.5
	LibSVM-2	Polynomial function kernel, gamma = 1.25, and c = 1.5
	LibSVM-3	Polynomial kernel with an exponent of 1
SMO	SMO-1	Polynomial kernel with an exponent of 1
	SMO-2	Pearson VII universal kernel with sigma and omega fixed to 1
NB	NB-1	We used this without a kernel estimation function
	NB-2	We used a kernel estimation function
RF	RF-1	The number of trees used was 10

4.5. Optimized CNN-Based Method

The performance of vision-based tasks has been greatly improved with deep learning techniques [46–51]. This paper introduces a deep learning method for the challenging task of liver disease classification. We use the concept of SIS in our work. We discuss the proposed method by using the idea of semantic segmentation (SS in this part of the paper).

Many factors greatly affect the performance of deep learning methods—for instance, the type of kernel used, the number of convolutional layers employed, the filter and its description, etc. We used different combinations of convolutional layers (CovLs). Each CovL was then followed by a maximum pooling layer (MPL). We checked various parameters and sizes of CovLs. Tables 4 and 5 present details of these parameters. For the activation function in the CovLs, we used a rectifier linear unit (RLU). We used three layers to construct a deep convolutional network, i.e., CovL, MPL, and FCL.

Table 4. Parameter settings for the CovL and MPL.

Type of Layer	Size of Stride	Feature Map	Size of Kernel	Output Size
Input	–	–	–	250×250
CovL1	2	96	5×5	124×124
MPL1	2	96	3×3	62×62
CovL2	2	256	5×5	30×30
MPL2	2	256	3×3	15×15
CovL3	2	316	5×5	12×12
MPL3	2	316	3×3	6×6
CovL4	2	512	5×5	4×4
MPL4	2	512	3×3	2×2

Table 5. Different parameter settings for the CNN training.

Parameter Used	Value Fixed
Epochs	150
Momentum	0.8
Batch size	250
Base learning rate	10^{-5}

4.5.1. Model Learning

Our proposed network is shown in Figure 4. We used a feature extraction framework (FEF) to extract the features of healthy and affected livers. The various stages in Figure 5 show the main blocks of the feature-learning part. In Figure 5, stage 1 handles the feature variations. In CT images, there are scaling variations due to certain environmental factors. These receptive fields overcome all of these variations. As is made clear in Figure 5, each field has 16 filters. The output from the first stage is then given to stage 2, which is an FCL. In stage 2, we use a 2×2 MPL to extract features. The RLU then follows each CovL. Between the CovL and FCL, we placed a Spatial Pyramid (SPd). The SPd produces an output that is given to the FCL in stage 3. Stages 3 and 4, which are shown in Figure 5, take care of the feature extraction. Finally, the last stage, stage 4, an FCL, extracts the final features, which are then given to the next module for SS. Various parameters can be studied in Tables 4 and 5.

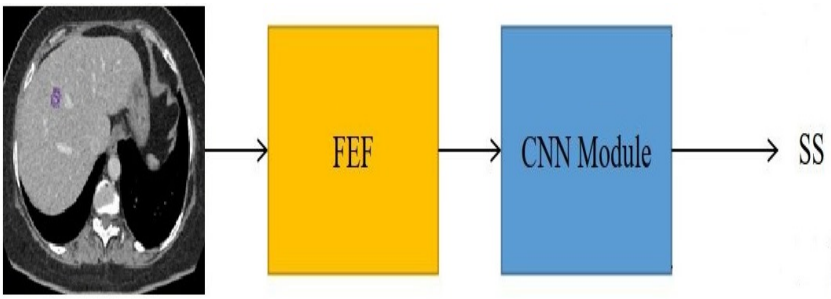

Figure 4. Proposed SIS-based liver disease classification model.

In the SIS part, the training data are given to the framework. We gave the results to the CovL, and they were extracted in the form of an estimated density and segmentation map. We introduced a loss into the model in the segmentation phase. For the density estimation functions, we used a Euclidean distance map.

4.5.2. CNN Optimization

Over-fitting is a severe problem that is faced mainly by machine learning models. To tackle this problem, we used the methodology suggested and used in [52]. We used four loss functions to optimize the network, including supervision loss. We also introduced a novel loss into the SS part of the framework. The loss was based on the Dice coefficient.

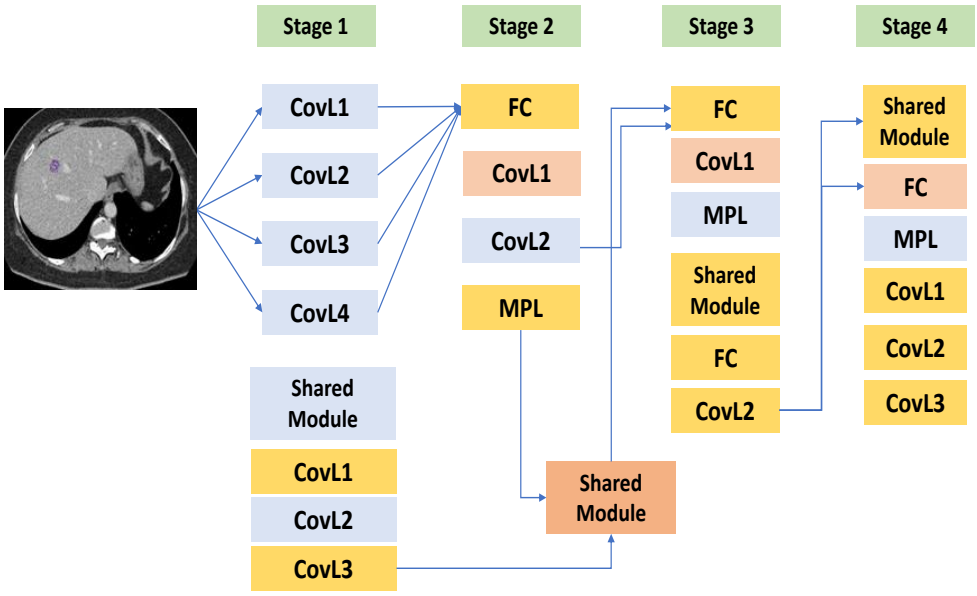

Figure 5. The proposed SIS-based model for the feature extractor framework.

5. Results and Discussion

This section presents details about the experimental setup and reports the results. This section also comprehensively explains the results obtained from the selection of various features and experiments. We tested the proposed method on 3000 images obtained through CT in 71 subjects. Some considerations that emerged from the experiments are summarized in the following paragraphs.

- We performed experiments using an Intel I-7 with 16 GB of RAM. We used an NVIDIA graphical processing unit with an 840 graphics card. We performed all experiments with TensorFlow and Keras. We used convolutional and maximum pooling layers. Details about these layers are summarized in Tables 4 and 5 and Figure 4.
- We evaluated our proposed model with the Precision (*PR*), Recall (*RC*), F1 measure (*FM*), and Accuracy (*AC*). In classification problems, the *FM* is frequently used to measure the performance of a method. The *FM* provides the weighted mean of two terms known as *PR* and *RC*. *AC* is used to measure the ability of a classifier to categorize all images in a dataset. When the *AC* value is high, the classifier's performance is good, and a low value indicates poor performance. *AC* is a single metric that reports the overall performance of a machine learning model. Mathematically, these terms can be represented as:

$$PR = \frac{(TP}{(FP) + (TP)} \tag{1}$$

$$RC = \frac{(TP)}{(FN) + (TP)} \tag{2}$$

$$FM = 2 * \frac{(PR) \times (RC)}{(PR) + (RC)} \tag{3}$$

$$AC = \frac{(TP + TN)}{(TP + TN + FN + FP)} \quad (4)$$

- We performed both 5-fold and 10-fold validation experiments in the proposed work. Comparatively better results were noted with the 10-fold cross-validation experiments; therefore, the results of only the 10-fold cross-validation experiments are reported in this paper. The result of the 10-fold cross-validation experiments are shown in Tables 6 and 7. The results for the F1 measure and Accuracy are only summarized in Tables 6 and 7.
- We observed that the choice of the feature used and its corresponding parameter settings mattered a lot. We used different configurations, and we noticed a big difference between the best and worst results. From Tables 4 and 5, it is clear that better results were shown by the LibSVM classifier. From both tables, it is clear that LibSVM in version 1 showed better results for the F1 measure and Accuracy. For LibSVM in version 1, we used a radial basis function kernel with the value of gamma fixed to 1.25, and the value of c was 1.5.
- We discussed various feature-ranking methods based on similarity and statistical knowledge and explained these methods in the section on the proposed method. These ranking methods included the information gain, gain ratio, and relief algorithm. It must be noted that these methods produce the same feature set by using the ranking criteria. We performed two kinds of experiments. We first used the extracted feature vector with a size of 37, and then performed experiments with the feature-ranking method discussed in the methodology section. We observed better results for the feature-ranking method instead of using texture features directly.
- To classify liver images, we employed various classifiers. Given five classes and a feature vector Z with an unknown label, the main target was to predict that Z was in one of the five classes. We designed two feature vectors for evaluating the performance of each classifier. The feature vector F1 consisted of all 37 features extracted in the feature extraction stage. The second feature vector, F2, consisted of the highest-ranked features selected based on similarity statistics and a knowledge-based ranking scheme. These features included the entropy, skewness, radial sum, information measure with correlation 1 and 2, and angular sum.
- All features extracted from images were combined in a vector known as F1. We employed k-fold validation experiments in this research. We kept the value of k = 5, and then used k = 10. In the cross-validation experiments, in the first iteration, $k - 1$ of the whole database was utilized for the training phase and was kept for testing. We reiterated the entire procedure k times and reported the average results in the paper for each classifier. The results reported in Tables 4 and 5 are for the cross-validation experiments with k = 10. From both Tables 4 and 5, it is clear that LibSVM-1 exhibited comparatively better results in the 10-fold experiments.
- It was observed that statistical techniques based on CT texture analysis showed excellent discrimination results for most liver abnormalities. There were 312 samples selected and used for liver tissue characterization. From this set of data, a total of 1209 regions of interest were designed from infected livers (liver abscess), 302 ROIs were added from metastatic livers, 1171 regions of interest were collected from liver necroses, and 304 were from abnormal vascular areas, while 224 regions of interest from normal liver data were used to compare with each type of abnormal liver data to make classes 1, 2, 3, 4, and 5. This work summarizes the texture analysis methods for liver categorization and tissue characterization using CT images.
- The values of the F1 measure that we found with the proposed SIS- and deep-learning-based method for classes 1, 2, 3, 4, and 5 were 1.0, 0.98, 0.98, 0.97, and 0.99, respectively. Similarly, the Accuracy reported for the SIS-based model for classes 1, 2, 3, 4, and 5 was 0.99, 1.0, 0.98, 0.97, and 0.99, respectively. The values reported for the F1 measure and accuracy with the deep-learning-based methods were much better than those for the conventional machine learning methods. However, we would like to add that some

papers on the topic reported that conventional machine learning that uses hand-crafted features shows better results than those of deep learning architectures. We would like to add that a better understanding of these methods is still needed to address CV-specific problems. For example, a condition of limited data may be something that deep-learning-based methods face, which is a significant drawback for deep learning architectures. From the published papers, our experiments, and the work on the topic, we observed that traditional machine learning techniques perform well with data collected in laboratory or indoor conditions. However, the performance drops considerably when these conventional methods are exposed to real-time scenarios. On the other hand, deep learning methods extract a comparatively higher level of abstraction. However, it is also true that the research community has some concerns about deep learning methods. For example, these methods are complicated and require inputs from the practitioner's end at various stages. In a nutshell, these algorithms are well engineered and much more time-consuming. However, it is also true that the only choice when implementing CV-based tasks is a deep-learning-based method.

Table 6. Results reported for the F1 measure.

Classifier	Class 1	Class 2	Class 3	Class 4	Class 5	Average
KNN-1	0.95	0.96	0.96	0.97	0.94	0.95
KNN-2	0.97	0.97	0.93	0.95	0.93	0.95
KNN-3	0.98	0.97	0.93	0.96	0.91	0.95
LibSVM-1	0.99	0.98	0.96	0.97	0.92	0.96
LibSVM-2	0.97	0.98	0.98	0.92	0.92	0.95
LibSVM-3	0.95	0.97	0.98	0.91	0.90	0.94
SMO-1	0.97	0.95	0.93	0.92	0.91	0.93
SMO-2	0.95	0.95	0.94	0.93	0.92	0.93
NB-1	0.92	0.94	0.95	0.94	0.91	0.93
NB-2	0.98	0.95	0.95	0.94	0.93	0.95
RF	0.99	0.95	0.93	0.92	0.91	0.94

Table 7. Results reported for Accuracy.

Classifier	Class 1	Class 2	Class 3	Class 4	Class 5	Average
KNN-1	0.96	0.94	0.95	0.92	0.91	0.93
KNN-2	0.96	0.93	0.92	0.91	0.90	0.92
KNN-3	0.98	0.95	0.94	0.93	0.93	0.94
LibSVM-1	0.97	0.97	0.96	0.99	0.97	0.98
LibSVM-2	0.98	0.94	0.97	0.98	0.93	0.96
LibSVM-3	0.99	0.95	0.95	0.96	0.94	0.95
SMO-1	0.97	0.93	0.96	0.92	0.93	0.94
SMO-2	0.95	0.97	0.96	0.94	0.94	0.95
NB-1	0.96	0.96	0.98	0.92	0.95	0.95
NB-2	0.97	0.94	0.96	0.98	0.92	0.95
RF	0.98	0.94	0.93	0.92	0.92	0.93

6. Conclusions

These techniques have revealed the variations in the texture patterns of normal and diseased livers. These results were a significant achievement in confirming the variation in liver texture from disease to disease, and even from mild to severe cases in a single disease. These methods are simpler to implement and easy to handle. We cannot speak of the perfection of a single method. The analysis can be varied from disease to disease. However, the combination of different techniques can provide promising results when discriminating different tissue textures. Future work should include the use of multiple types of analytic software to confirm the clinical outcomes and set a standardization. Suitable training is necessary for the generation of consistent diagnostic reports and implementing these approaches. In conclusion, we could show that texture analysis of CT images is a practically independent method that may help classify different liver stages from normal to abnormal. This study shows that abnormalities that appear in the human liver can be

distinguished and diagnosed by using texture analysis techniques, which may assist radiologists and medical physicists in predicting the severity and proliferation of abnormalities in liver diseases.

Author Contributions: Investigation, methodology, resources M.N.; project administration, resources, software S.A.B.; funding acquisition, writing-review & editing, validation conceptualization, formal analysis, Writing draft K.K., and visualization, validation M.S.A. All authors have read and agreed to the published version of the manuscript.

Funding: This research received no external funding.

Conflicts of Interest: The authors declare no conflict of interest.

References

1. Denbow, D.M. Gastrointestinal Anatomy and Physiology. In *Sturkie's Avian Physiology*, 6th ed.; Academic Press: Cambridge, MA, USA, 2015; pp. 337–366.
2. WHO. *Global Health Estimates 2015: Deaths by Cause, Age, Sex, by Country and by Region*; WHO: Geneva, Switzerland, 2015.
3. Rahimian, J.; Wilson, T.; Oram, V.; Holzman, R.S. Pyogenic liver abscess: Recent trends in etiology and mortality. *Clin. Infect. Dis.* **2004**, *39*, 1654–1659. [CrossRef] [PubMed]
4. Akhondi, H.; Sabih, D. Liver Abscess. 2021. Available online: https://www.ncbi.nlm.nih.gov/books/NBK538230/ (accessed on 15 October 2021).
5. Burt, A.; Ferrell, L.; Hubscher, S. *MacSween's Pathology of the Liver E-Book*; Elsevier Health Sciences: Amsterdam, The Netherlands, 2017.
6. Pere, G.; Graupera, I.; Lammert, F.; Angeli, P.; Caballeria, L. Screening for liver fibrosis in the general population: A call for action. *Lancet Gastroenterol. Hepatol.* **2016**, *1*, 236–264.
7. Anthony, P.P.; Ishak, K.G.; Nayak, N.C.; Poulsen, H.E.; Scheuer, P.J. The morphology of Cirrhosis. Recommendations on definition, nomenclature and classification by a working group sponsored by the World Health Organization. *J. Clin. Pathol.* **1978**, *31*, 395–414. [CrossRef] [PubMed]
8. Goldfarb, G.; Nouel, O.; Poynard, T.; Rueff, B. Efficiency of respiratory assistance in cirrhotic patients with liver failure. *Intensive Care Med.* **1983**, *9*, 271–273. [CrossRef] [PubMed]
9. Garcia-Doval, I.; Hernandez, M.V.; Vanaclocha, F.; Sellas, A.; Montero, D. Should tumor necrosis factor antagonist safety information be applied from patients with rheumatoid arthritis to psoriasis? Rates of serious adverse events in the prospective rheumatoid arthritis BIOBADASER and psoriasis BIOBADADERM cohorts. *Br. J. Dermatol.* **2017**, *176*, 643–649. [CrossRef] [PubMed]
10. Hossein, A.; Sabih, D.E. Liver Abscess. 2019. Available online: https://europepmc.org/article/NBK/nbk538230 (accessed on 15 October 2021).
11. Scheuer, J.H. *Liver Biopsy Interpretation E-Book*; Elsevier Health Sciences: Amsterdam, The Netherlands, 2020.
12. Siriwardena, K.; Mason, J.M.; Mullamitha, S.; Hancock, H.C.; Jegatheeswaran, S. Management of colorectal cancer presenting with synchronous liver metastases. *Nat. Rev. Clin. Oncol.* **2014**, *8*, 446–459. [CrossRef] [PubMed]
13. Azer, S.A. Deep learning with convolutional neural networks for identification of liver masses and hepatocellular carcinoma: A systematic review. *World J. Gastrointest. Oncol.* **2019**, *12*, 1218–1230. [CrossRef]
14. Xu, J.; Jing, M.; Wang, S.; Yang, C.; Chen, X. A review of medical image detection for cancers in digestive system based on artificial intelligence. *Expert Rev. Med. Devices* **2019**, *10*, 877–889. [CrossRef]
15. Faust, O.; Acharya, U.R.; Meiburger, K.M.; Molinari, F.; Koh, J.E. Comparative assessment of texture features for the identification of cancer in ultrasound images: A review. *Biocybern. Biomed. Eng.* **2018**, *2*, 275–296. [CrossRef]
16. Moghbel, M.; Mashohor, S.; Mahmud, R.; Saripan, M.I.B. Review of liver segmentation and computer assisted detection/diagnosis methods in computed tomography. *Artif. Intell. Rev.* **2018**, *4*, 497–537. [CrossRef]
17. Nayantara, P.V.; Kamath, S.; Manjunath, K.; Rajagopal, K. Computer-aided diagnosis of liver lesions using CT images: A systematic review. *Comput. Biol. Med.* **2020**, *3*, 234–248. [CrossRef]
18. Kaur, R.; Juneja, M.; Mandal, A.K. A hybrid edge-based technique for segmentation of renal lesions in CT images. *Multimed. Tools Appl.* **2018**, *6*, 12917–12937. [CrossRef]
19. Jeffers, A.M.; Sieh, W.; Lipson, J.A.; Rothstein, J.H.; McGuire, V. Breast cancer risk and mammographic density assessed with semiautomated and fully automated methods and BI-RADS. *Radiology* **2016**, *2*, 348–355. [CrossRef] [PubMed]
20. Muthuselvan, S.; Rajapraksh, S.; Somasundaram, K.; Karthik, K. Classification of Liver Patient Dataset Using Machine Learning Algorithms. *Int. J. Eng. Technol.* **2018**, *7*, 323–326. [CrossRef]
21. Idris, K.; Bhoite, S. Applications of Machine Learning for Prediction of Liver Disease. *Int. J. Comput. Appl. Technol. Res.* **2019**, *8*, 394–396. [CrossRef]
22. Murty, S.V.; Kumar, R.K. Enhanced classifier accuracy in liver disease diagnosis using a novel multi layer feed forward deep neural network. *Int. J. Recent Technol. Eng.* **2019**, *8*, 1392–1400.

23. Murty, S.V.; Kumar, R.K. Accurate Liver Disease Prediction with Extreme Gradient Boosting. *Int. Eng. Adv. Technol.* **2019**, *8*, 2288–2295.
24. Ali, U.; Shaukat, A.; Hussain, M.; Ali, J.; Khan, K.; Khan, M.B.; Shah, M.A. Automatic cancerous tissue classification using discrete wavelet transformation and support vector machine. *J. Basic Appl. Sci. Res.* **2016**, *6*, 15–23.
25. Joloudari, J.H.; Saadatfar, H.; Dehzangi, A.; Shamshirb, S. Computer aided decision-making for predicting liver disease using PSO-based optimized SVM with feature selection. *Inform. Med. Unlocked* **2019**, *17*, 100255. [CrossRef]
26. Wu, J.-H.; Wei, W.; Zhang, L.; Wang, J.; Damaševičius, R.; Li, J.; Wang, H.-D.; Wang, G.-L.; Zhang, X.; Yuan, J.-X.; et al. Risk assessment of hypertension in steel workers based on LVQ and fisher-SVM deep excavation. *IEEE Access* **2019**, *7*, 23109–23119. [CrossRef]
27. Aljarah, I.; Al-Zoubi, A.M.; Faris, H.; Hassonah, M.A.; Mirjalili, S.; Saadeh, H. Simultaneous Feature Selection and Support Vector Machine Optimization Using the Grasshopper Optimization Algorithm. *Cogn. Comput.* **2018**, *10*, 478–495. [CrossRef]
28. Chao, C.-F.; Horng, M.-H. The Construction of Support Vector Machine Classifier Using the Firefly Algorithm. *Hindawi Publ. Corp. Comput. Intell. Neurosci.* **2015**, *8*, 212719. [CrossRef] [PubMed]
29. Askarzadeh, A. A novel metaheuristic method for solving constrained engineering optimization problems: Crow search algorithm. *Comput. Struct.* **2016**, *169*, 1–12. [CrossRef]
30. Singh, M.; Singh, S.; Gupta, S. An information fusion-based method for liver classification using texture analysis of ultrasound images. *Infect. Fusion* **2014**, *3*, 91–96. [CrossRef]
31. Chen, C.H. *Handbook of Pattern Recognition and Computer Vision*; World Scientific: Singapore, 2015.
32. Zayed, S.; Elnemr, H.A. Statistical analysis of haralick texture features to discriminate lung abnormalities. *J. Biomed. Imaging* **2015**, *5*, 356–369. [CrossRef] [PubMed]
33. Chang, C.C.; Chen, H.H.; Chang, Y.C.; Yang, M.Y.; Lo C.M.; Ko, W.C.; Lee, Y.F.; Liu, K.L.; Chang, R.F. Computer-aided diagnosis of liver tumors on computed tomography images. *Comput. Methods Programs Biomed.* **2017**, *5*, 45–51. [CrossRef] [PubMed]
34. Chen, C.H.; Chang, C.K.; Tu, C.Y.; Liao, W.C.; Wu, B.R.; Chou, K.T.; Chiou, Y.R.; Yang, S.N.; Zhang, G.; Huang, T.C. Radiomic features analysis in computed tomography images of lung nodule classification. *PLoS ONE* **2018**, *5*, e0192002. [CrossRef]
35. Wei, G.; Cao, H.; Ma, H.; Qi, S.; Qian, W. Content-based image retrieval for lung nodule classification using texture features and learned distance metric. *J. Med. Syst.* **2018**, *1*, 42. [CrossRef]
36. Kuo, W.J. Computer-aided Diagnosis for feature Selection and Classification of Liver Tumors in Computed Tomography Images. In Proceedings of the IEEE International Conference on Applied System Invention, Chiba, Japan, 13–17 April 2018; pp. 1207–1210.
37. Balodi, A.; Dewal, M.L.; Anand, R.S.; Rawat, A. Texture based classification of the severity of mitral regurgitation. *Comput. Biol. Med.* **2016**, *1*, 157–164. [CrossRef]
38. Manth, N.; Virmani, J.; Kumar, V.; Kalra, N.; Khandelwal, N. Application of Texture Features for Classification of Primary Benign and Primary Malignant Focal Liver Lesions. In *Image Feature Detectors and Descriptors*; Springer: Cham, Switzerland, 2016; pp. 385–409.
39. Li, J.; Cheng, K.; Wang, S.; Morstatter, F.; Trevino, R.P.; Tang, J.; Liu, H. Feature selection: A data perspective. *ACM Comput. Surv.* **2018**, *2*, 50. [CrossRef]
40. Delzell, D.A.; Peter, T.; Smith, M.; Magnuson, S. Machine learning and feature selection methods for disease classification with application to lung cancer screening image data. *Front. Oncol.* **2019**, *9*, 22. [CrossRef] [PubMed]
41. Khan, K.; Ahmad, N.; Ullah, K.; Din, I. Multiclass semantic segmentation of faces using CRFs. *Turk. J. Electr. Eng. Comput. Sci.* **2017**, *25*, 3164–3174. [CrossRef]
42. Yu, H.; Scalera, J.; Khalid, M. Texture analysis as a radiomic marker for differentiating renal tumors. *Abdom. Radiol.* **2017**, *3*, 12. [CrossRef]
43. Lee, H.S.; Hong, H.; Jung, D.C. Differentiation of fat-poor angiomyolipoma from clear cell renal cell carcinoma in contrast enhanced MDCT images using quantitative feature classification. *Med Phys.* **2014**, *3*, 3604–3614. [CrossRef]
44. Khan, K.; Ahmad, N.; Khan, F.; Syed, I. A framework for head pose estimation and face segmentation through conditional random fields. *Signal Image Video Process.* **2020**, *14*, 159–166. [CrossRef]
45. Patacchiola, M.; Cangelosi, A. Head pose estimation in the wild using convolutional neural networks and adaptive gradient methods. *Pattern Recognit.* **2017**, *3*, 132–143. [CrossRef]
46. Voulodimos, A.; Doulamis, N.; Doulamis, A.; Protopapadakis, E. Deep learning for computer vision: A brief review. *Comput. Intell. Neurosci.* **2018**, *2018*, 7068349. [CrossRef]
47. Akhtar, N.; Mian, A. Threat of adversarial attacks on deep learning in computer vision: A survey. *IEEE Access* **2018**, *6*, 14410–14430. [CrossRef]
48. Pradhyumna, P.; Shreya, G.P. Graph Neural Network (GNN) in Image and Video Understanding Using Deep Learning for Computer Vision Applications. In Proceedings of the 2021 Second International Conference on Electronics and Sustainable Communication Systems (ICESC), Coimbatore, India, 4–6 August 2021; pp. 1183–1189.
49. Sinha, R.K.; Pandey, R.; Pattnaik, R. Deep learning for computer vision tasks: A review. *arXiv* **2018**, arXiv:1804.03928.
50. Varadi, R.; Naik, U.P. Quantum Convolutional Neural Networks (QCNN) Using Deep Learning for Computer Vision Applications. In Proceedings of the 2021 International Conference on Recent Trends on Electronics, Information, Communication & Technology (RTEICT), Bangalore, India, 27–28 August 2021; pp. 728–734.

51. Niall, O.M.; Campbell, S.; Carvalho, A.; Harapanahalli, S.; Hernandez, G.V.; Krpalkova, L.; Riordan, D.; Walsh, J. Deep learning vs. traditional computer vision. In *Science and Information Conference*; Springer: Cham, Switzerland, 2019; pp. 128–144.
52. Collobert, R.; Jason, W. A unified architecture for natural language processing: Deep neural networks with multitask learning. In Proceedings of the 25th International Conference on Machine Learning, Helsinki, Finland, 5–9 July 2008; pp. 160–167.